Electropolymerization of pyrrole-tailed imidazolium ionic liquid for the elaboration of antibacterial surfaces

Hamdi Ben Halima,[1] Thibaut Zwingelstein,[2] Vincent Humblot,[2] Boris Lakard,[1] Lydie Viau[1]*

[1] Institut UTINAM, UMR CNRS 6213, 16 Route de Gray, Université Franche-Comté, 25030 Besançon, France

[2] Université Franche-Comté, UMR CNRS 6174, Institut FEMTO-ST, 15B avenue des Montboucons, 25030 Besançon, France

ABSTRACT

A strategy was developed to prepare antibacterial surfaces by electropolymerization of a pyrrole-functionalized imidazolium ionic liquid bearing an halometallate anion. The objective was to combine the antibacterial efficiency of polypyrrole with those of the ionic liquid components (cation and anion). For this, the pyrrole-functionalized imidazolium monomer [PyC_8MIm]Br was synthesized and coordinated to $ZnCl_2$. The antibacterial properties of the pyrrole-functionalized imidazolium monomers with bromide and the halometallate anion were evaluated against *E. coli* and *S. aureus* by measurement of their minimum inhibitory concentration (MIC) values. Surprisingly, different trends were observed. Against *E. coli* a decrease in MIC values was observed upon the incorporation of $ZnCl_2$ while an increase in MIC values was obtained against *S. aureus*. Mixtures of pyrrole and the pyrrole-functionalized ionic liquid were then used for the electrodeposition of polypyrrole films on Fluoride doped Tin Oxide (FTO) substrates. The films were carefully characterized by X-ray Photoelectron Spectroscopy (XPS), water contact angle measurements, profilometry, and Scanning Electron Microscopy (SEM). The antibacterial activity of the polypyrrole-films was determined both by disk diffusion method and by the colony forming units (CFU) counting method over time. Films obtained by incorporation of the pyrrole-functionalized imidazolium monomer with halometallate anion showed excellent antibacterial properties, much higher than those of polypyrrole alone which validate our strategy. Furthermore, the antibacterial properties were much higher against Gram-positive than against Gram-negative bacteria. Finally, the antibacterial performances over time were tuned by the concentration of the pyrrole-functionalized ionic liquid monomer used.

KEYWORDS

Antibacterial, polypyrrole, ionic liquid, electropolymerization

INTRODUCTION

Since the early 2000's Ionic liquids (ILs) have been used for biomedical applications[1] such as protein stabilization,[2] nanocarriers, biosensing, for the solubilization of drugs, in drug delivery[3] and as antimicrobial agents.[4, 5] Their antibacterial properties have been attributed to electrostatic forces between the cationic ILs component and the negatively charged bacteria membranes that led to the localization of the cation close to the membrane. Furthermore, hydrophobic interactions between the ILs alkyl chains and the cellular lipids cause the insertion of the cation into the membrane. These two kinds of interactions constitute the basis of the two mechanisms proposed for ILs antibacterial properties *i.e.* the insertion of the hydrophobic part of the IL into the cell membrane causes the release of cytoplasmic content and the change of the membrane charges' surface leads to aggregation of bacterial cells and the inhibition of bacterial growth.[6, 7] Thus, the antibacterial properties of ILs can be modulated by a proper choice of the alkyl chain lengths and the nature of the cations and anions. There are only few reports on the use of halometallate ILs *i.e.* species formed by combining a metal halide and an organic halide salt for biomedical applications even though many metal salts are Generally Recognized As Safe (GRAS). In 2012, Del Sesto and collaborators reported the first example on the use of chlorometallate ILs, especially $ZnCl_2$-based ones, for pharmaceutical formulations that present antibiofilm activity.[8] Other examples include those of Gilmore *et al.* on the study of 1-alkyl-3-methylimidazolium tetrachlorocuprate(II) and dibromoargentate(I) ILs that present enhanced antimicrobial activity when compared to their chlorinated analogues[9] and of de la Fuente-Nunez *et al.* who report good antibacterial properties with low toxicity towards human cells of the surfactant dodecyltrimethylammonium bromotrichloroferrate.[10]

Several Poly(Ionic Liquids) (PILs), especially cationic ones, have also been developed for antibacterial applications.[11] These polymers that contain ILs side groups combine the advantages of the antibacterial properties of ILs with polymer processability. Especially, the group of Yan and collaborators have studied the antibacterial properties of different polycationic and polyanionic PILs membranes formed from imidazolium-based or pyrrolidinium-based monomers that bear different anions. This team has also investigated the antibacterial properties of PILs membranes containing metal salts as anions and demonstrated that these anions have more effect on the antibacterial properties than the modification of the chemical structure of the cation.[12, 13] ILs and PILs have also been grafted on surface to elaborate antibacterial surfaces. Examples in this field include the

functionalization of titania particles,[14] of polyethersulfone and polydimethylsiloxane[15] membranes,[16] of gold,[17] stainless steel[18] and silicon surfaces.[19]

On the other hand, Conjugated Polymers (CPs) have demonstrated great potentials in biomedical applications in particular in tissue engineering, biosensing, drug delivery, bioactuators and implantable medical devices.[20-22] Among the various CPs for biomedical applications, polypyrrole (PPy) is probably the most widely studied due to its good biocompatibility.[23] PPy is also known to present antibacterial properties against Gram-negative[24] and Gram-positive bacteria[25, 26] and these properties can be enhanced by incorporation of silver ions.[27-29] PPy can be obtained by chemical oxidation or electropolymerization of pyrrole monomers.[30]

Pyrrole-tailed imidazolium compounds have been used previously for the preparation of different materials such porous materials[31] and PILS.[32] The electropolymerization of these pyrrole-tailed imidazolium constitutes an alternative strategy to graft ILs on surfaces. To our knowledge only three papers have used this strategy to prepare conductive PPy films[33, 34] that can be used for solid-phase microextraction.[35]

Here, our objective is to elaborate antibacterial surfaces that combine the antibacterial properties of the biocompatible polypyrrole with those of an IL. For this, our strategy relies on the electropolymerization of a pyrrole-functionalized imidazolium IL that bears metal salt as anion that can be regarded as safe. The antibacterial properties of our surfaces were tested against Gram-negative *Escherichia coli* (*E. coli*) and Gram-positive *Staphylococcus aureus* (*S. aureus*) bacteria by means of both agar diffusion and killing assays.

EXPERIMENTAL SECTION

Materials and chemicals.

The chemicals used were obtained from the following commercial sources: Pyrrole and NaH from Acros Organics; 1,8- dibromooctane from Alfa-Aesar, *N*-methylimidazole, zinc chloride ($ZnCl_2$), acetonitrile, toluene, dichloromethane and methanol from sigma Aldrich; *N*-[3-(trimethoxysilyl)propyl]pyrrole (TMSP) was purchased from abcr; the culture media Mueller Hinton (MH) broth, Lysogeny broth Miller (Luria-Bertani) and PBS Merck-Sigma-Aldrich The rectangular-shaped FTO substrates (15 mm x 30 mm, thickness: 1.1 mm, R =

80 Ω/square) were purchased from Solems. Dry dimethylformamide (DMF) was obtained by a solvent purification system PureSolve MD5 from Innovative Technology. Preparative purifications were performed by silica gel flash column chromatography (Teledyne CombiFlash EZ PREP UV/ELSD HPLC Flash Chromatography). Solvents used as eluents were of technical grade.

Instrumentation.

Infrared Spectra. For each sample, 128 infrared scans were recorded with a 4 cm^{-1} resolution on a Bruker vertex70 FTIR spectrometer equipped with a DGTS detector using a Platinum ATR accessory equipped with a diamond crystal.

NMR. The ^{1}H and ^{13}C NMR spectra were obtained on a Bruker AVANCE 400 HD instrument. ^{1}H chemical shifts were referenced to the proton impurity of the NMR solvent and ^{13}C chemical shifts to the NMR solvent.

Water contact angles of the modified and unmodified FTO substrates were measured using a GBX Scientific Instruments contact angle analyzer (Digidrop Contact Angle Meter used with Windrop software) with 2 µL water drops with a dosing rate of 0.58 µL/s. The drop was formed on the tip of a syringe needle and placed onto the sample surface by raising the sample until contact was made. Contact angles were determined by drawing the tangent close to the edge of the droplet. For each sample, at least 5 measurements were performed.

Mechanical Profilometry The thickness (T) and roughness of PPy (100 mM) + pyrrole-functionalized Ionic Liquid [PyC_8MIm]Br-$ZnCl_2$ at 5 mM and 100 mM films were measured by profilometry using a stylus (2.5 µm)-based mechanical probe profiler Alpha-Step IQ from KLA Tencor. Arithmetic roughness (Ra) was measured on a scan length of 3000 µm at a scan speed of 100 $\mu m \cdot s^{-1}$. Since the deposition did not cover the entire FTO substrate, the thickness (T) of the sample could be measured, in the same operating conditions, using the step at the deposition/substrate interface. Reported Ra and T are the means of at least 5 measurements done at different places of the samples.

GDOES spectroscopy. Glow Discharge Optical Emission Spectroscopy was used since it combines sputtering and atomic emission to provide qualitative depth profiles. GDOES analyses were performed in radio frequency mode with a GD Profiler from JobinYvon Horiba. After optimization, the parameters used for the erosion of the polymer films were: a flush time (time to obtain pure argon atmosphere inside analysis chamber) of 30 s, a pressure

of 400 Pa, and a power of 40 W. The wavelengths of the spectral lines used were 130.217 nm (oxygen), 156.144 nm (carbon), 288.158 nm (silicon), 149.262 nm (nitrogen), and 317.505 nm (tin). Carbon, nitrogen and silicon elements were used to follow the TMSP layer; tin, oxygen, and silicon elements were used to follow the substrate since FTO is composed of a thin layer of tin oxide deposited onto a silicon oxide surface.

SEM microscopy. The surface morphology of the pure polypyrrole film, the PPyZn-5 and PPyZn-100 films were obtained, without metallization treatment, using a high-resolution scanning electron microscope Thermo Scientific Apreo 2 with an electron beam energy of 5 keV.

XPS. Chemical surface analyses of the samples were studied on a Versaprobe 5000 spectrometer (ULVAC-PHI, Inc.) equipped with a monochromatized and a focalized Al Kα X-ray source (1486.6 eV). For each sample, survey spectra, as well as high-resolution core-level region of C1s, N1s, O1s, Zn2p, Cl2p, Br3d levels, were acquired over a spot size of 200 µm. To record the survey spectra and high-resolution regions, pass energies of 187.5 eV and 58.7 eV were used, respectively. Data processing was done using Casa XPS software[36] and energy calibration was done on C1s CC/CH bonds at 284.8 eV. The quantification was obtained from the measurement of the corresponding peak area and the use of relative sensitivity factors (RSF), specific of the spectrometer and furnished by the manufacturer.

Synthesis.

Synthesis of *N*-Bromooctyl pyrrole PyC_8Br.

1,8-dibromooctane (12.16 g, 44.7 mmol), was dissolved at 0 °C in 100 mL of dry DMF. In another flask, pyrrole (2.00 g, 29.8 mmol), was added to a cooled suspension (0°C) of NaH (60 %wt) (1.31 g, 32.7 mmol) in dry DMF (100 mL). The resulting mixture was allowed to reach room temperature and stirred for 30 min then cooled again to 0 °C. The resulting solution was poured into the 1,8-dibromooctane solution by canula. The mixture was allowed to reach room temperature and stirred for 24 h. The resulting solution was hydrolyzed by the addition of water and the product was extracted with EtOAc (3×100 mL). The resulting organic phase was washed with water (3×100 mL), dried over Na_2SO_4, filtered, and the solvent was removed under vacuum. The resulting compound was purified by chromatography on silica gel using CombiFlash (eluent: dichloromethane/Cyclohexane,

1:9). PyC_8Br was obtained as a transparent oil (4.4 g, 57%). ^{1}H NMR (400 MHz, $CDCl_3$): δ = 6.65 (t, J = 2.1 Hz, 2H, H_2), 6.14 (t, J = 2.1 Hz, 2H, H_1), 3.87 (t, ^3J = 7.1 Hz, 2H, H_3), 3.40 (t, ^3J = 6.8 Hz, 2H, H_{10}), 1.85 (qt, ^3J = 6.8 Hz, 2H, H_9), 1.76 (qt, ^3J = 6.8 Hz, 2H, H_4), 1.42 (qt, ^3J = 6.8 Hz, 2H, H_8), 1.29 (m, 6H, H_5, H_6, H_7). ^{13}C {^{1}H} NMR (100.6 MHz, $CDCl_3$): δ = 120.5 (C2), 107.9 (C1), 49.7 (C3), 34.0 (C10), 32.8 (C9), 31.6 (C4), 29.1 (C6), 28.7 (C7), 28.1 (C8), 26.7 (C5) ppm. IR (ATR): 2927, 2854, 1499, 1461, 1357, 1280, 1087, 1060, 967, 717, 644, 616, 560 cm^{-1}.

Synthesis of the Pyrrole-functionalized imidazolium [PyC_8MIm]Br.

PyC_8Br (4 g, 15.5 mmol) was dissolved in 70 mL of toluene before the addition of *N*-methylimidazole 1.53 g (18.6 mmol). The resulting mixture was refluxed for 24 h. After cooling down to room temperature, two phases were formed. The lower phase that contained the product was washed several times with diethyl ether (3×50 mL) and the solvent was evaporated under vacuum. The final product [PyC_8MIm]Br was recovered as a white solid (4.90 g, 93%). mp = 89-91°C. ^{1}H NMR (400 MHz, $CDCl_3$): δ = 10.70 (s, 1H, H_{13}), 7.30 (bt, 1H, H_{12}), 7.23 (bt, 1H, H_{11}), 6.63 (t, J = 2.1 Hz, 2H, H_2), 6.12 (t, J = 2.1 Hz, 2H, H_1), 4.30 (t, ^3J = 7.5 Hz, 2H, H_{10}), 4.11 (s, 3H, H_{14}), 3.85 (t, ^3J = 7.5 Hz, 2H, H_3), 1.90 (bqt, 2H, H_9), 1.74 (bqt, 2H, H_4), 1.32 (m, 8H, H_5, H_6, H_7, and H_8). ^{13}C{^{1}H} NMR (100.6 MHz, $CDCl_3$): δ = 137.5 (C13), 123.7 (C12), 120.0 (C11), 120.5 (C2), 107.8 (C1), 50.1 (C10), 49.6 (C3), 36.8 (C14), 31.5 (C4), 30.3 (C9), 28.8/28.9 (C6/C8), 26.6 (C5), 26.1 (C7) ppm. IR (ATR): 3084, 3038, 2933, 2849, 1559, 1503, 1463, 1438,1426, 1385, 1336, 1278, 1155, 1095, 1052, 970, 869, 841, 782, 744, 731, 709, 659, 625 cm^{-1}.

Synthesis of the metal-containing Pyrrole-functionalized imidazolium [PyC_8MIm]Br-$ZnCl_2$.

Equal molars of [PyC_8MIm]Br (1g, 2.94 mmol) and anhydrous $ZnCl_2$ (400 mg, 2.94 mmol) were mixed and stirred in methanol (8 mL) at room temperature for 24 h. The desired compound was obtained after evaporation of methanol under vacuum.[13] [PyC_8MIm]Br-$ZnCl_2$ was obtained as a yellowish viscous oil (1.39 g, 99%). ^{1}H NMR (400 MHz, $CDCl_3$): δ = 8.95 (s, 1H, H_{13}), 7.38 (bt, 1H, H_{12}), 7.28 (bt, 1H, H_{11}), 6.65 (t, ^3J = 2.0 Hz, 2H, H_2), 6.09 (t, ^3J = 2.0 Hz, 2H, H_1), 4.22 (t, ^3J = 7.5 Hz, 2H, H_{10}), 3.98 (s, 3H, H_{14}), 3.84 (t, ^3J = 7.5 Hz, 2H, H_3), 1.83 (bqt, 2H, H_9), 1.72 (qt, ^3J = 7.2 Hz, 2H, H_4), 1.29 (m, 8H, H_5, H_6, H_7, and H_8). ^{13}C {^{1}H} NMR (100.6 MHz, $CDCl_3$): δ = 136.1 (C13), 124.0 (C12), 122.3 (C11), 120.7 (C2), 107.8 (C1), 50.3 (C10), 49.7 (C3), 37.4 (C14), 31.6 (C4), 30.2 (C9), 28.9 (C6/C8),

26.6 (C5), 26.2 (C7) ppm. IR (ATR): 3315, 3143, 3107, 2929, 2856, 1567, 1500, 1458, 1373, 1279, 1163, 1089, 1063, 1006, 832, 727, 649, 619 cm^{-1}. ESI+ m/z : 260.21 $[PyC_8MIm]^+$, . m/z (ESI$^-$): 168.83 $[ZnCl_3]^-$,212.78 $[ZnCl_2Br]^-$, 258.73 $[ZnBr_2Cl]^-$, 302.68 $[ZnBr_3^-]$, 330.15 $[(PyC_8MIm)Cl_2]^-$, 374.09 $[(PyC_8MIm)ClBr]^-$ 420.04 $[(PyC_8MIm)Br_2]^-$.

Silanization of FTO substrate by TMSP.

Silanization of FTO substrates was performed according to the procedure described by Sougueh *et al*.[37] FTO substrates were immersed into 20 mL of Toluene to which was added 0.2 mL of TMSP. The resulting solution was refluxed for 24 hours under nitrogen atmosphere. The thus obtained TMSP-FTO substrates were rinsed several times with dichloromethane followed by drying in air.

Electrochemistry.

All electrochemical experiments were performed with a SP-200 potentiostat from Biologic at room temperature (20 ± 2 °C). The instrument was controlled by a PC computer via EC-Lab V11.43 software interface. Electrochemical experiments were performed using a three-electrode setup with FTO substrates (4.5 cm^2) or platinum wire (area 0.785 mm^2) as working electrodes, a Saturated Calomel Electrodes (SCE) reference electrode and a platinum sheet as counter-electrode.

The cyclic voltammetry technique was applied to perform the electropolymerization on platinum electrode of acetonitrile solutions containing either 5 mM of the pyrrole monomer or 5 mM $[PyC_8MIm]Br\text{-}ZnCl_2$ + 100 mM $LiClO_4$ in the potential range from -0.7V/SCE to 1.6V/SCE with a scan rate of 100 mV/s.

Polypyrrole films were then electrodeposited on TMSP-FTO by chronoamperometry at +1.5 V/SCE for 900s. Different films were obtained depending on the concentration of the monomers used. The monomers solutions prepared in acetonitrile contain all 50 mM pyrrole and 5, 10, 50 or 100 mM of $[PyC_8MIm]Br\text{-}ZnCl_2$. The resulting polypyrrole films are named according to the following PPyZn-X where X represents the $[PyC_8MIm]Br\text{-}ZnCl_2$ monomer concentration. Five films have been prepared, namely, PPy, PPyZn-5, PPyZn-10, PPyZn-50 and PPyZn-100 (Table 1).

Table 1. Nomenclature of the synthesized polypyrrole films with the concentrations of monomers used (mM).

	PPy	PPyZn-5	PPyZn-10	PPyZn-50	PPyZn-100
Pyrrole	50	50	50	50	50

$[PyC_8MIm]Br\text{-}ZnCl_2$	0	5	10	50	100

After deposition and rinsing with acetonitrile, the polymer films were analyzed using profilometry, SEM microscopy, XPS and contact angle measurements.

Electrochemical Impedance Spectroscopy (EIS) measurements were performed using an electrochemical cell consisting of three electrodes. The reference electrode was a saturated calomel electrode, the auxiliary electrode was a platinum sheet and the modified-FTO substrates were used as working electrode. EIS measurements were carried out in the presence of the redox probe $[Fe(CN)_6]^{3-}/[Fe(CN)_6]^{4-}$ at 5 mM in PBS buffer at pH 7.4, with a frequency ranged from 100 kHz to 1 Hz, two frequency points per frequency decade, and using a modulation voltage of 10 mV (Eac). During the measurements, the potential was kept at 0.2 V (Edc) versus the SCE reference. Data fitting on EIS spectra was performed with Randomize (5000 iterations) + Simplex method (fit stopped on 5000 iterations) and the following equivalent circuit model $[R_1 + Q_2/ R_{ct}]$ where R_1 is the electrolyte solution's resistance ($[Fe(CN)_6]^{3-/4-}$), the parallel elements are Q_2 (the coefficient of the constant phase element), and R_{ct} (the charge transfer resistance).

Antibacterial properties.

Bacterial strains and growth conditions.

Microbiological experiments were conducted with Gram-negative *Escherichia coli (E. coli* ATCC 25922) and Gram-positive *Staphylococcus aureus* (*S. aureus* ATCC 25923). Bacteria were stored at -80°C in culture media-glycerol aliquots. Before the experiments, they were incubated overnight at 30°C on Lysogeny Broth (Miller-LB, 20 $g.L^{-1}$) agar (15$g.L^{-1}$) plate for *E. coli* and at 37°C on Mueller-Hinton (MH, 25$g.L^{-1}$) agar (15$g.L^{-1}$) plate for *S. aureus*. Then, a liquid pre-culture was prepared with one colony of *E. coli* or *S. aureus* in LB or MH media, respectively, and stirred overnight (90 rpm) at 30°C or 37°C. Bacterial concentration in liquid culture was estimated via UV-Vis spectroscopy (UV-2450 Shimadzu spectrophotometer) at 620 nm using a calibration curve. At this stage, the initial bacterial concentration is close to 10^9 $CFU.mL^{-1}$.

Minimal Inhibition Concentration (MIC) measurements.

MICs values were determined by the two-fold dilution method. Experiments were performed in 96-well microplates as triplicate in culture media (LB for *E. coli* and MH for *S. aureus*), with an initial bacterial concentration of approximately 10^6 $CFU.mL^{-1}$. The highest

concentrations were prepared in distilled water. These concentrations were then two-fold serially diluted with broth. After overnight incubation at 30°C/37°C, MICs were determined as the lowest concentration of the compound with no visible bacterial growth. Sterility control (culture broth only), growth control (culture broth with bacteria) and death control (culture broth with bacteria and 50% ethanol) assessed the quality of each experiment.

Inhibition zone assays.

For the inhibition zone assay, the disk diffusion method was used. Films were placed on *E. coli* or *S. aureus* Mueller–Hinton agar plates at an inoculum concentration of 10^6 CFU/mL and then the plates were incubated at 30 or 37 °C overnight.

Time-killing assays.

Suspensions of *E. coli* in LB and *S. aureus* in MH Bacteria with initial concentration close to 10^9 CFU.mL^{-1} were centrifuged (5000×g, 5 min, 4°C). The supernatant was removed and replaced by the same quantity of PBS. This process was performed twice to remove any trace of media culture. The bacterial suspensions were diluted in PBS to obtain a concentration of 10^6 CFU.mL^{-1}. The films electropolymerized on FTO substrates were placed in a sterile 6-wells plate. 5 mL of a bacterial suspension were added and the plates were incubated at 30°C or 37°C in an orbital oven at 90 rpm. Aliquots of 100 µL were taken of the suspensions at different times, serially diluted in LB or MH. The number of CFUs were determined by plate inoculation in spiral mode on LB/agar or MH/agar Petri dishes using Interscience EasySpiral automatic inoculator. After overnight incubation at 30°C or 37°C, respectively for *E. coli* and *S. aureus*, the CFUs were enumerated with a Interscience Colony Counter Scan 300. Controls were run without films. The number of CFUs were used to calculate the percentage of killing efficacy.

RESULTS AND DISCUSSION

Synthesis of the pyrrole-tailed monomer

Scheme 1 shows the synthetic procedure used to prepare the pyrrole-functionalized imidazolium ionic liquid used in this study. This procedure implies three steps. The first two steps were adapted from what we reported recently.[38] Briefly, Pyrrole was *N*-alkylated by reaction with 1,8-dibromooctane in the presence of NaH to afford PyC_8Br. This compound

was quaternized using *N*-Methyl imidazole to afford the brominated imidazolium compound [PyC_8MIm]Br. ILs containing bromine anions are well known for their antibacterial properties however, as observed previously by other authors, the electropolymerization of this brominated compound did not form polymeric films.[33, 35] As mention in the introduction, some halometallates ILs and PILs that present antibacterial properties have been reported. Especially, Yan and collaborator have studied the activity of PILs membranes coordinated with $CuCl_2$, $FeCl_3$ and $ZnCl_2$.[13] The $CuCl_2$-containing membrane presented the highest antibacterial activity among the three metals. Our attempt to prepare the halometallate ILs by reaction of [PyC_8MIm]Br with $FeCl_3$ and $CuCl_2$ did not afford the expected metal-containing IL monomers but formed brown precipitates of polypyrrole. Indeed, $FeCl_3$ and, to a lesser extent $CuCl_2$, are well known oxidizing agent used for the chemical polymerization of pyrrole.[39, 40] With thus choose to work with Zn^{2+} ions whose antibacterial properties are well known.[41] The halometallate ionic liquid [PyC_8MIm]Br-$ZnCl_2$ was prepared by the equimolar reaction of [PyC_8MIm]Br with $ZnCl_2$ in methanol ($\chi ZnCl_2 = 0.5$).[13] The structural characterization of the final compound [PyC_8MIm]Br-$ZnCl_2$ was confirmed by ^1H, ^{13}C and IR spectroscopy. The speciation of halometallate anions has already been studied by different technics.[42-46] Here, the final compound was analyzed by mass spectrometry. As expected, the most intense peak in the positive mode corresponds to the molecular peak of the cation $[PyC_8MIm]^+$ while, in the negative mode, the most intense peak was m/z 212 corresponding to $[ZnCl_2Br]^-$. The other peaks have been attributed to clusters containing $[ZnCl_yBr_z]^-$ or $[(PyC_8MIm)Cl_yBr_z]^-$ species. Dinegative ions are absent in the mass spectra. The study by Seddon and collaborators has however shown that mass spectrometry analysis can only confirm the presence of monocharged specie in the gas phase and not in the liquid phase.[42] Licence and coworkers have studied by X-Ray photoelectron spectroscopy (XPS) of the IL [C_8MImCl]-$ZnCl_2$ and evidenced the presence of $[Zn_2Cl_6]^{2-}$ anions for $\chi ZnCl_2$=0.5.[46] The speciation of the anion measured by XPS will be discussed in the characterization part of the films (see below).

Scheme 1: Synthesis of the pyrrole-functionalized imidazolium used in this study.

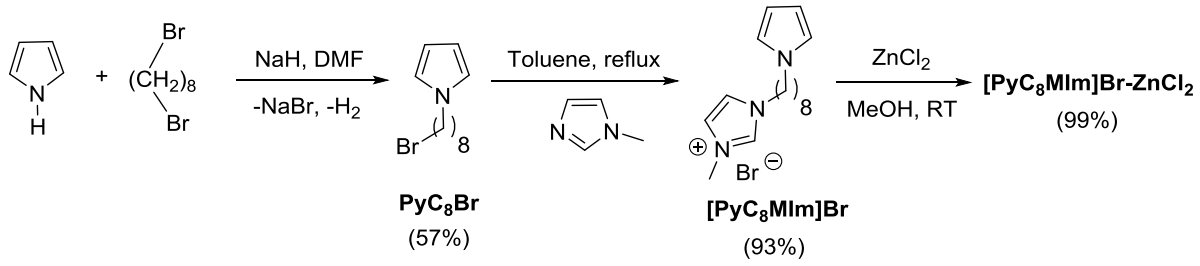

Description of the procedure used in this study.

With the pyrrole-functionalized imidazolium monomer in hands, we then turn to the electropolymerization of this monomer on FTO substrates. The general procedure used in this study is described in Scheme 2. Before electropolymerization, fluorine-doped tin oxide (FTO) substrates were first organosilanized using *N*-[3-(trimethoxysilyl)propyl]pyrrole (TMSP). This step was proven to be necessary to improve the adherence of our polymer on the FTO substrate. The electropolymerization was then performed in the presence of a mixture of pyrrole (0.05 M) and [PyC_8MIm]Br-$ZnCl_2$ at various concentrations (5, 10, 50 and 100 mM) (see experimental section for the nomenclature of the films). The use of a mixture of each monomer was also proven to be necessary as our attempts to electropolymerize the monomer [PyC_8MIm]Br-$ZnCl_2$ alone also led to poor adhesion of the films when dipped in Phosphate Buffer Saline (PBS) solutions. The antibacterial properties of the pyrrole-functionalized imidazolium monomer [PyC_8MIm]Br-$ZnCl_2$ were evaluated by determination of the Minimum Inhibitory Concentration (MIC) and the antibacterial activities of the resulting polypyrrole films were then studied by the agar disk diffusion method and time killing assays.

Scheme 2. Global synopsis of the study.

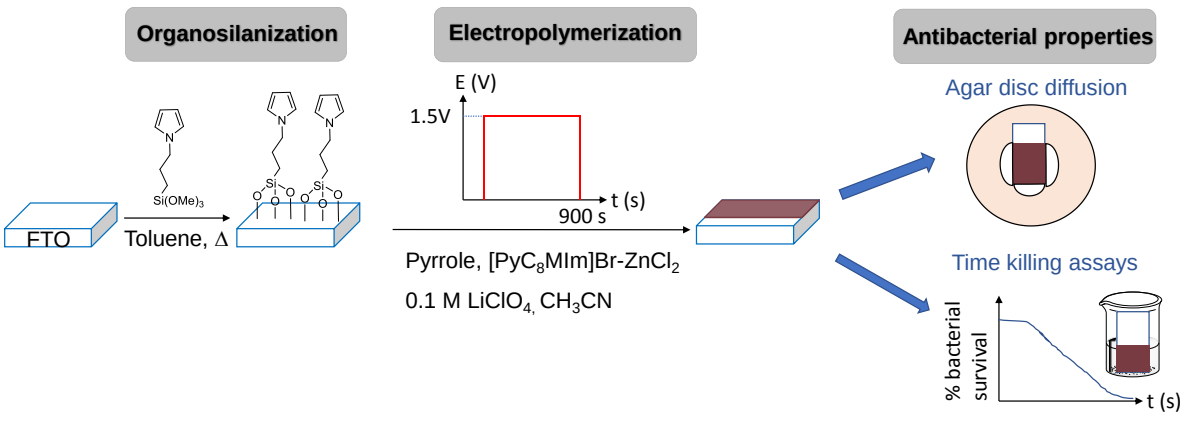

Organosilanization of FTO substrates.

In order to improve the adherence of the polypyrrole films, we used a method developed by some of us that has been successfully applied to enhance the adherence of polypyrrole films.[37] This method consists in the organosilanization of FTO substrates using a trimethoxysilane bearing a pyrrole function *i.e.* using TMSP. The functionalization is performed in refluxing toluene overnight under nitrogen atmosphere. The efficiency of the organosilanization was confirmed by different technics: electrochemistry, XPS measurements and GDOES analysis. Our results are in accordance with those previously described[37] and are only briefly summarized here.

Cyclic voltammetry was performed using bare FTO or TMSP-modified FTO substrates as working electrode in a solution of acetonitrile containing 0.1 M $LiClO_4$. Difference between the two voltammograms evidences the appearance of a peak at +1.15V/SCE due to the oxidation of the pyrrole moiety (Figure 1). Also, the XPS survey spectrum presents peaks associated to Si and N at Binding Energy of 102.4 and 401.0 eV, respectively, that also confirms the presence of the pyrrole-functionalized silane on the FTO substrate (Figure 2).

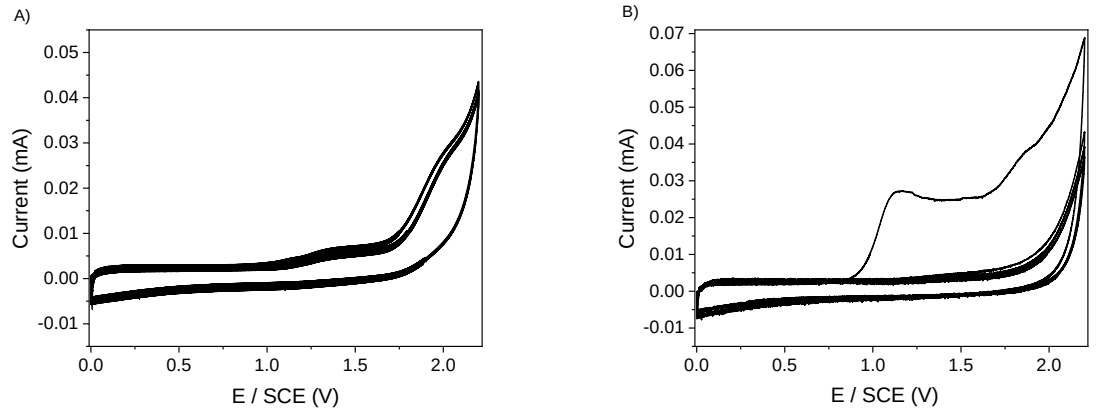

Figure 1. Cyclic voltammograms of (A) bare FTO electrode and (B) TMSP-modified FTO electrode recorded in CH_3CN solution containing 0.1 M $LiClO_4$.

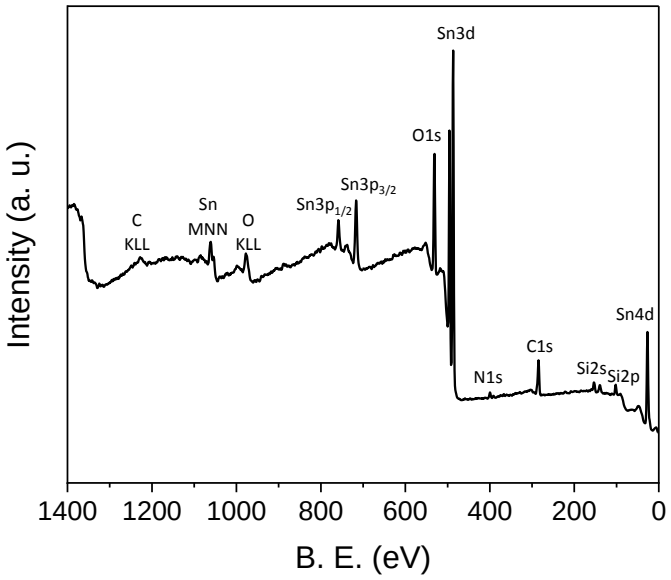

Figure 2. XPS survey spectrum of TMPS-modified FTO.

Compared to the bare FTO, the GDOES profile of the TMSP-FTO substrate presents at the beginning of the erosion, an increase of the carbon and nitrogen signals characteristics to the presence of the propyl pyrrole function and of the silicon signal attributed to the presence of the silyl group (Figure 3).

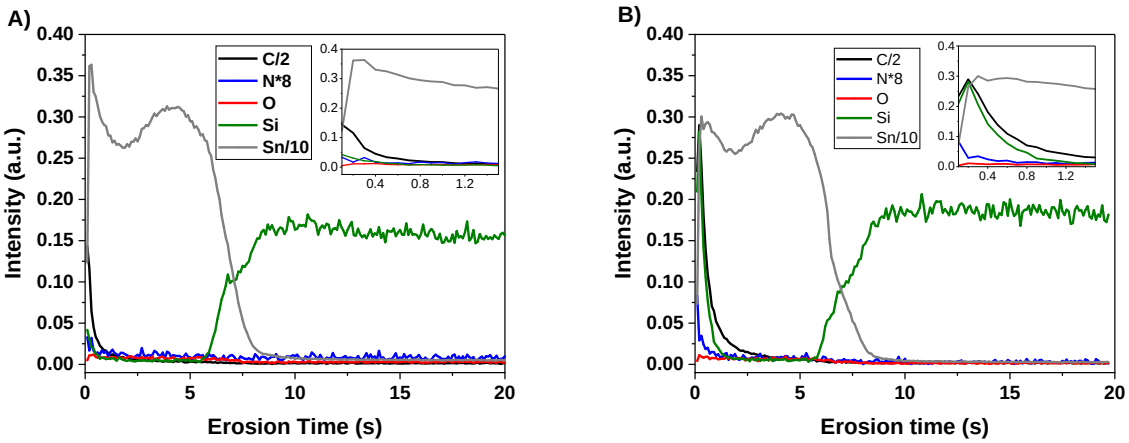

Figure 3. Glow Discharge Optical Emission Spectroscopy depth profile of A) bare FTO substrate B) organosilanized FTO substrate.

Electrochemical deposition of polypyrrole films.

Electropolymerization using cyclic voltammetry.

The electrochemical deposition of pyrrole and [PyC_8MIm]Br-$ZnCl_2$ monomers were first performed using cyclic voltammetry. The cyclic voltammogram (CV) obtained for the pyrrole monomer (Figure 4) presents a peak at about + 1.2 V/SCE characteristic to the oxidation of the pyrrole monomer that initiates the electrochemical polymerization.[47] Following scans also show this monomer oxidation peak, but also oxidation and reduction peaks characteristics of the polypyrrole oxidation and reduction which appear around +0.2V/SCE and 0.0 V/SCE, respectively. The CV obtained using [PyC_8MIm]Br-$ZnCl_2$ also presents a peak at +1.2V/SCE in the second scan due to the oxidation of the pyrrole moiety. The intensity of this peak is slightly lower than in the case of pyrrole indicating the formation of a slightly less conductive film. The peak attributable to the reduction of polypyrrole is located at -0.1V/SCE.

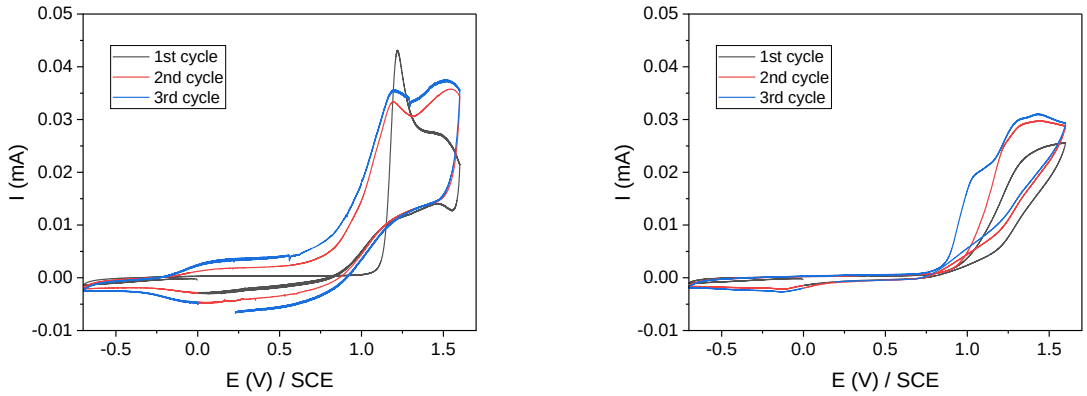

Figure 4. Potentiodynamic growth of polypyrrole films in (left) 5 mM solution of pyrrole + 0.1 M $LiClO_4$ in acetonitrile (right) 5 mM [PyC_8MIm]Br-$ZnCl_2$ + 0.1 M $LiClO_4$ in acetonitrile Scan rate: 100 mV/s. Working electrode: platinum wire.

Electropolymerization using Chronoamperometry.

After that, different acetonitrile solutions containing the same pyrrole (50 mM) and $LiClO_4$ (100 mM) concentrations , but different [PyC_8MIm]Br-$ZnCl_2$ concentrations (100, 50, 10 or 5 mM) were prepared. Chronoamperometry technique was used to perform the electro-oxidation of these solutions on FTO substrates by applying a potential of +1.5V/SCE during 15 min. Black solid films were observed in all cases confirming that the electropolymerization has been successfully performed. As examples, Figure 5 presents the current-time plots obtained using the highest and lowest concentrations *i.e.* 100 mM and 5 mM of [PyC_8MIm]Br-$ZnCl_2$. The current intensity sharply increased before leveling off.

This increase is due to the nucleation process related to the oxidation of pyrrole monomers into radical cations whereas the plateau corresponds to the polymer growth.[48] It should be pointed out that no decay versus time was observed as should be the case if overoxidation of the polymer had occurred. As expected, the current intensity is highest for the sample PPyZn-100. The ratio between the total electric charges Q_{100}/Q_5 obtained during films growth is equal to 1.2 (Eq. 1):

$$Q_{100}/Q_5 = I_{100}*t_{100}/I_5*t_5 = I_{100}/I_5 = 7.4/6.15 = 1.2 \qquad \text{(Eq. 1)}$$

Where the indexes 100 and 5 stand for the samples PPyZn-100 and PPyZn-5, respectively.

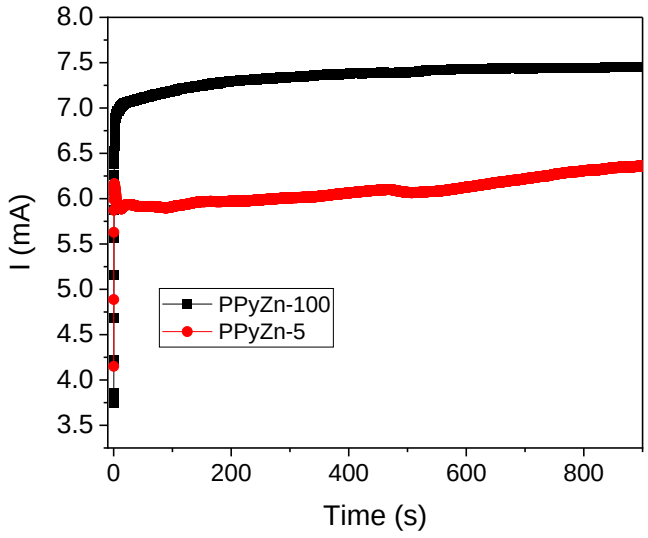

Figure 5. Current intensity-time plots in the presence of 0.05 M pyrrole + $[PyC_8MIm]Br$-$ZnCl_2$ at 100 mM (black) and 5 mM (red) at +1.5V/SCE.

Physico-chemical characterization of the films

XPS survey spectra of PPyZn-5 and PPyZn-100 films revealed the presence of C1s, N1s, O1s, Cl2p, Zn2p and Br3d components as can be seen in Table 2 and Figure 6. For comparison, data obtained for the electropolymerization of an acetonitrile solution of pyrrole in 0.1 M $LiClO_4$ are also reported in Table 2. The presence of oxygen elements in all samples is due to the incorporation of ClO_4^- as doping agents during the electropolymerization of pyrrole, confirmed by the presence of Cl2p component in the survey spectra.[47] As expected by the low content of $[PyC_8MIm]Br$-$ZnCl_2$ in PPyZn-5 film,

the atomic percentages obtained for Br (0.2%) and Zn (0.2%) are low. These atomic percentages increased to 5.5% (Zn) and 3.7% (Br) with a rise of [PyC_8MIm]Br-$ZnCl_2$ content in PPyZn-100. At a first sight, it might be surprising that the chlorine content remains almost the same between PPyZn-5 and PPyZn-100. As the oxygen content decreases about two times when the amount of [$PPyC_8MImBr$]-$ZnCl_2$ is increased, it means that the amount of ClO_4^- has decreased. Thus, the decrease of chloride content coming from the perchlorate has been compensated by incorporation of more chloride from $ZnCl_2$.

Table 2. XPS data (binding energy (BE) and atomic percent) for PPyZn-5, PPyZn-100 and PPy films.

	PPyZn-5		**PPyZn-100**		**PPy**	
Components	Peak BE (eV)	Atomic %	Peak BE (eV)	Atomic %	Peak BE (eV)[47]	Atomic %[47]
C1s	284.6	59.4	284.8	62.8	284.7	68.3
N1s	400.2	11.2	401.3	10.7	400.0	7.7
O1s	532.2	24.1	532.1	12.0	532.2	20.5
Cl2p	207.3	4.9	198.7	5.3	207.7	3.5
$Zn2p_{3/2}$	1022.2	0.2	1022.4	5.5	-	-
Br3d	683.0	0.2	68.9	3.7	-	-

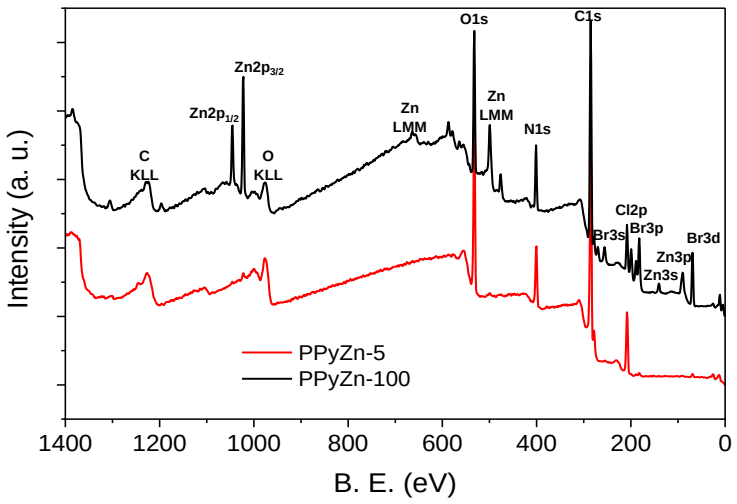

Figure 6. Comparison of the XPS survey spectra of PPyZn-5 and PPyZn-100 films.

Figure 7 shows comparison of the high resolution XPS spectra of the N1s core level peaks of PPyZn-5 and PPyZn-100. These peaks were fitted with two components, one at ca 400.0 eV and one at ca 401.5 eV. It has been shown that the N1s spectra of polypyrrole contains two components, one at 400.0 eV corresponding to the amine like structure (-NH-) and one at 401.8 eV corresponding to N-H+and =N-H+structures.[47] At the same time, XPS spectrum of imidazolim cations present a N1s peak at ca 401.5 eV[49, 50] overlapping with one of the N1s peak of polypyrrole. The ratios' intensities between the components at 401.5 eV and 400.0 eV are 0.6 and 1.9 for PPyZn-5 and PPYZn-100, respectively (Table 3). These values can be compared to the one reported for polypyrrole that is equal to 0.2.[47] Thus, an increase of the ratio clearly illustrated the incorporation of the imidazolium-functionalized pyrrole into the films. As expected, this ratio is more important in the case of PPyZn-100 film.

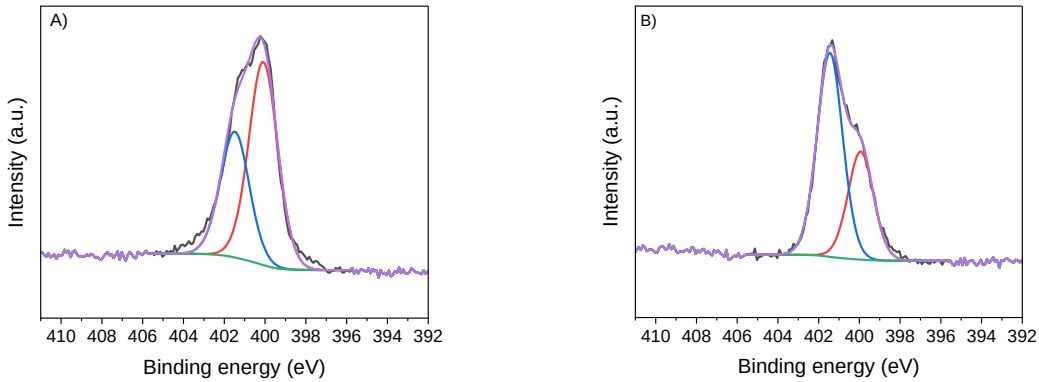

Figure 7. High resolution N1s XPS spectra of A) PPyZn-5 and B) PPyZn-100.

Table 3. Assignments of the peaks present in the XPS N1s spectra (binding energy and atomic %) of electrodeposited PPy films.

Sample	Peak BE (eV)	Atomic %	Assignment
PPy[47]	400.0	82.8	N-H
	401.8	17.2	$N{=}H^+$ and $N\text{-}H^+$
PPyZn-5	400.1	61.7	N-H
	401.5	38.3	$N{=}H^+$, $N\text{-}H^+$, N_{cation}
PPyZn-100	399.9	34.6	N-H
	401.4	65.4	$N{=}H^+$, $N\text{-}H^+$, N_{cation}

The shape and position of the Cl2p photoelectron peaks has been used to study the speciation of tetrachlorozincate(II) anions in imidazolium-based ILs.[46] The high resolution

XPS spectra of the Cl2p core level peaks of PPyZn-100 is reported in Figure 8. The Cl2p spectrum indicates the presence of three Cl ($2p_{1/2}$, $2p_{3/2}$) doublets. Each doublet is fitted by a $2p_{3/2}$:$2p_{1/2}$ intensity ratio of 2:1. The $Cl2p_{3/2}$ peak located at 207.6 eV is attributed to the ClO_4^- anions.[51] The two other doublets at 199.2 and 198.4 eV are attributed to bridging and terminal Cl atoms. The energy difference between these two chlorine atoms in different chemical environments are 0.7-0.8 eV in accordance with previous results.[46] The ratio of teminal:bridging Cl atoms is 1:1.5 (Table 4). This value indicated the presence of polynuclear $[Zn_nCl_{2n+1}Br]^{2-}$ anions.

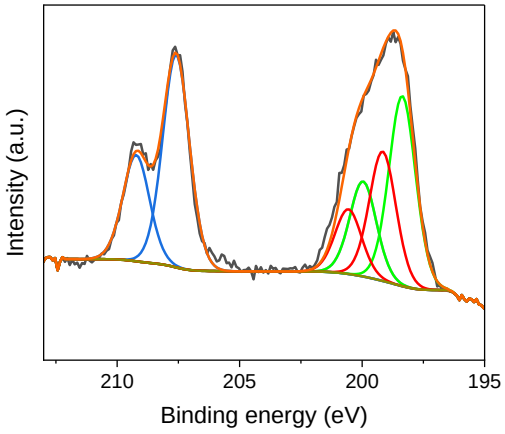

Figure 8. High resolution Cl2p XPS spectra of PPyZn-100.

Table 4. Assignments of the peaks present in the XPS Cl2p spectra (binding energy and atomic %) of PPyZn-100.

Peak BE (eV)	Atomic %	Assignment
209.2	13.3	$2p_{1/2}$ ClO_4^-
207.6	26.6	$2p_{3/2}$ ClO_4^-
200.6	8.1	$2p_{1/2}$ bridging Cl
199.2	16.2	$2p_{3/2}$ bridging Cl
199.9	11.9	$2p_{1/2}$ terminal Cl
198.4	23.8	$2p_{3/2}$ terminal Cl

Electrochemical impedance spectroscopy (EIS) is a nonstationary technique that allows the analysis of complex electrochemical systems. Figure 9, illustrates the Nyquist diagrams

of the bare FTO, the TMSP-FTO and the PPyZn-5-FTO surface in the presence of the redox probe $[Fe(CN)_6]^{3-}/[Fe(CN)_6]^{4-}$ at 5 mM in PBS buffer at pH 7.4. The charge transfer resistance (R_{ct}) values on the surface of the electrode surface were determined after fitting (see experimental section). After organosilanization of FTO with TMPS the R_{ct} value increases from 1090 Ω to 1716 Ω implying a high electron transfer resistance to the redox-probe and the blocking of charge transfer which can be explained by the non-conductive behavior of TMSP. Following electropolymerization, the PPyZn-5 film presents a very low R_{ct} value of 37Ω which accounts for the enhanced conductivity of the polypyrrole film.[52]

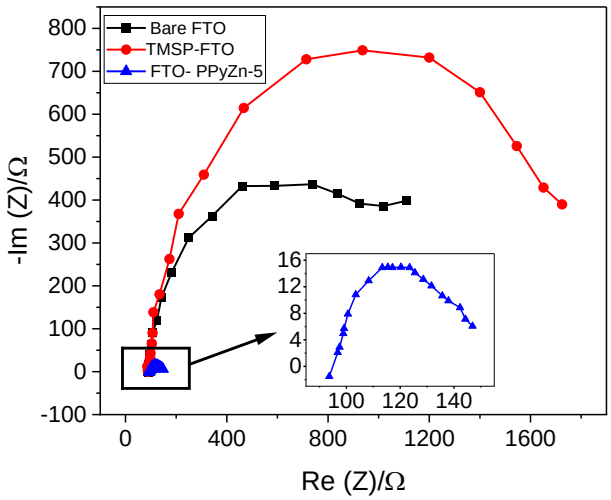

Figure 9. Nyquist plot obtained after the different steps of the functionalization. bare FTO (Black), FTO + TMSP (Red), FTO + TMSP + $[PyC_8MIm]Br\text{-}ZnCl_2$ 5 mM (blue) in 5 mM $[Fe(CN)_6]^{3-/4-}$ in PBS buffer, EIS frequency ranged from 100 KHz to 1 Hz, with Eac = 10mV and Edc = +0.2V/ ECS.

The morphology of the resulting polypyrrole films was observed by scanning electron microscopy (Figure 10). As discussed before in the chronoamperometry part, the electropolymerization of pyrrole begins with the formation of small nodules on the surface of the substrate, then the polymer continues to grow from the aggregation of these small nodules. The structure of the film PPyZn-5 presents a homogeneous surface composed of small aggregates of polypyrrole nodules of few nanometers. This structure is consistent with those reported previously in acetonitrile.[47] When the concentration of $[PyC_8MIm]Br\text{-}ZnCl_2$ is increased to 100 mM (PPyZn-100 film), bigger polypyrrole aggregates are formed that are surrounded by the alkyl imidazolium non-conductive organic component. The PPyZn-100

film is slightly thicker (x_{100} =8.9 μm) than the PPyZn-5 one (x_5 = 7.4 μm) and is also slightly rougher (Table 5). Interestingly, the Faraday's law is usually used to estimated films thicknesses *x* from the electrical charge (Q) according to equation (2):

$$x = \frac{QM}{\rho AzF} \qquad \text{(Eq. 2)}$$

Where M is the molar mass of pyrrole (67.09 $gmol^{-1}$), Q the electric charge, A the working electrode area, ρ the density of polypyrrole (1.5 $g.cm^{-3}$), z the number of electrons exchanged (2.25) and F the Faraday constant (95000 $C.mol^{-1}$).

According to this law, the ratio x_{100}/x_5 should be equal to Q_{100}/Q_5.
The ratio x_{100}/x_5 in our case is equal to 1.2 which corresponds to the value of Q_{100}/Q_5 found previously (see vide infra).

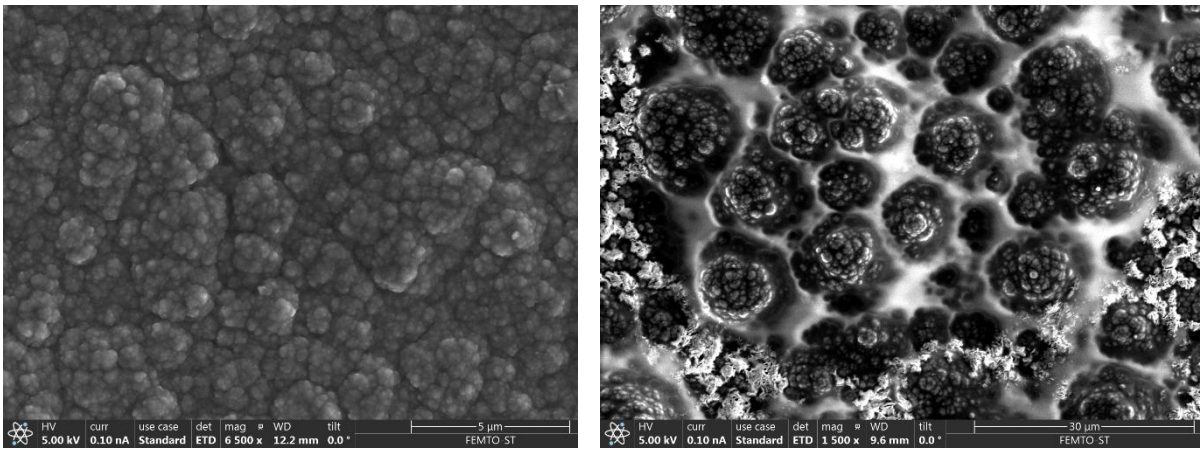

PPyZn-5 **PPyZn-100**

Figure 10. SEM micrographs of PPy films.

Table 5. Thickness and average roughness of the polypyrrole films grown in the presence of 50 mM pyrrole and different concentrations of $[PyC_8MIm]Br\text{-}ZnCl_2$.

Films	T (μm)	Ra (μm)
PPyZn-5	7.4±0.4	0.4±0.2
PPyZn-100	8.9±0.2	0.7±0.3

To further assess the effectiveness of the functionalization and the polymerization, water contact angle measurements were performed on bare FTO, TMSP-FTO and after electropolymerization. For bare FTO, a contact angle of 74.3 ± 3° was found as excepted

from the hydrophobic nature of the bare FTO. After grafting the TMSP on FTO substrates, the contact angle increased to 105.6 ± 2.0°. This hydrophobic character can be explained by the presence of TMSP hydrocarbon chains. Following electropolymerization, the contact angle decreased to 46.8 ± 1° for the PPyZn-5 film due to the hydrophilic nature of the halometallated imidazolium component. With an increase of the concentration of this component, the water contact angle further decreased to 32.3 ± 2.0° for the PPyZn-100 film (Table 6).

Table 6. Drop Water contact angle (WCA) results in degree obtained on the different surfaces.

Samples	FTO	TMSP-FTO	PPyZn 5mM	PPyZn 100mM
WCA (°)	74.3 ± 3.0	105.6 ± 2.0	46.8 ± 1.0	32.3± 2.0

Antibacterial properties

Several authors have studied the antibacterial properties of ILs focusing on the influence of the alkyl chain length,[53] the nature of the cationic head group or the nature of the anion. The main outlines are that longer alkyl chains led to the higher antibacterial properties until a cut off is reached after which the antibacterial efficiency decreased. The nature of the hydrophilic head group has no real influence on antibacterial properties[54] while the nature of anions does have influence, but this influence is small compared to the one of the alkyl chain lengths.[4] Some authors have also linked the antibacterial properties of ILs with their surface activity[55] and demonstrated good linear relationships between the antibacterial efficacy and the CMC for both imidazolium and pyridinium based ILs.[54] Recently, we have investigated the surfactant properties of the compound [PyC_8MIm]Br and found that it has slightly lower CMC and higher adsorption efficiency than its parent [C_8MIm]Br analogue. This has been attributed to the elongation of the alkyl chain length and π- π interactions among the pyrrole moieties. However, we also found that addition of a pyrrole function at the end of the alkyl chain does not lead to the same effect as addition of a methyl group on the Gibbs energy of aggregation (ΔG^0_m) due to the lower hydrophobicity of the pyrrole function.[38]

The antibacterial activity of the monomer [PyC_8MIm]Br-$ZnCl_2$ was first investigated by determination of its MIC against Gram-negative bacteria *E. coli* and Gram-positive bacteria *S. aureus*. These two microorganisms belong to important human and animal pathogens and

have been chosen as representatives of the main groups of infectious agents. Table 7 compares the MIC values obtained for $[C_8MIm]Br$, the same pyrrole functionalized IL $[PyC_8MIm]Br$ and the pyrrole-functionalized IL bearing the halometallate anion $[PyC_8MIm]Br\text{-}ZnCl_2$. All MIC values are below the CMCs meaning that the compounds are interacting in the form of monomer with cells ant not as aggregates. In the case of the Gram-positive *S. aureus* bacteria, the antibacterial efficiency increases with the incorporation of the pyrrole moiety with MIC values decreasing from 0.34 $\mu mol.mL^{-1}$ to 0.23 $\mu mol.mL^{-1}$ and by coordination to $ZnCl_2$ (MIC = 0.098 $\mu mol.mL^{-1}$). This higher efficiency might be attributed in the first case to the increase liphophilicity upon elongation of the alkyl chain length and, in the second case, to the formation of reactive oxygen species (ROS) such as singlet oxygen ($^1O_2$) by the zinc ions.[12] To our surprise, the opposite trend was observed with *E. coli*. MICs measurements were performed several times to verify this observation. Examples of reverse trend between the efficacity against Gram-positive and Gram-negative are quite rare. Recently, in the case of diketopyrrolopyrrole-based ILs, a non-monotonous effect of the increase of the alkyl chain lengths on the antibacterial activities was observed towards Gram-negative *E. coli*. The molecular sizes of these ILs greatly affected their membrane penetration and disruption abilities and thus. However, these authors also demonstrated that in the case of a Gram-positive bacteria of *Bacillus subtilis* all ILs penetrate the bacterial membrane whatever the alkyl chain length leading to good antibacterial properties.[56] The reason responsible for such differences is yet unclear but the results show different interaction process of these ILs against Gram-negative and Gram-positive bacteria. Guzmán and collaborators also studied the antibacterial activity of *N*-alkylimidazolium salts functionalized with *p*-coumaric or cinnamic acid. They found that the salts having a hydroxyl groups in their structure (*p*-coumaric derivatives) have better antibacterial activities against Gram-positive bacteria than the salts with no hydroxyl groups while, on the contrary they present lower antibacterial activity (higher MICs values) against Gram-negative bacteria. The reason is also unclear but might be due to the differences in the cell-wall between the two types of bacteria.[57] Indeed, Gram-negative bacteria are surrounded by an additional lipopolysaccharide membrane that protects them against antibacterial agents. In our study, in all cases , the antibacterial activity was better against Gram-positive *S. aureus* compared to Gram-negative *E. Coli* bacteria in accordance with previous reports.[58, 59] However, these tendencies should be considered with caution as Weyhing-Zerrer *et al* have shown that bactericidal efficacy could not be generalized across strains of bacteria, even within the same Gram category.[60]

Table 7. Comparison of MIC and CMC values for studied compounds.

Compound	*E. coli* ATCC 25922		*S. aureus* ATCC 25923		CMC
	$\mu g.mL^{-1}$	$\mu mol.mL^{-1}$	$\mu g.mL^{-1}$	$\mu mol.mL^{-1}$	$(mmol.mL^{-1})$
$[C_8MIm]Br$	375	1.36	93.75	0.34	160[54]
$[PyC_8MIm]Br$	640	1.88	80.00	0.23	87[38]
$[PyC_8MIm]Br\text{-}ZnCl_2$	1000	2.10	46.87	0.098	nd

nd: non determined

The antibacterial properties of our films on FTO substrates were then evaluated qualitatively by inhibition zone assays. For both bacteria we investigated films containing different concentrations of $[PPyC_8MIm]Br\text{-}ZnCl_2$ and compared the results with the film containing only polypyrrole and with the silane-modified FTO substrate (TMSP-FTO). As all the films containing polypyrrole or substituted-polypyrrole are highly opaque we focus the results on the formation of a halo resulting from diffusion and contact killing. A seen in Figure 11, for *E. coli* some halos are visible on the agar plates obtained with samples PPy-100 and PPy-50 containing the highest amounts of $[PyC_8MIm]Br\text{-}ZnCl_2$ while the PPy and PPy-10 films do not present any halos. These halos are much more important on agar plates containing *S. aureus* even for the film elaborated with a starting concentration of 10 mM of $[PyC_8MIm]Br\text{-}ZnCl_2$ (PPyZn-10). For *S. aureus*, we also studied the film PPyZn-5 but in this case no specific halo was observed. From these images we can qualitatively conclude that our polypyrrole-functionalized imidazolium $ZnCl_2$ films have good antibacterial properties and that their antibacterial efficiency is higher towards *S. aureus* while polypyrrole films do not present much activity. The highest activity found for our films against *S. aureus* is in good accordance with the data obtained from MIC measurements on the $[PyC_8MIm]Br\text{-}ZnCl_2$ monomer.

E. coli

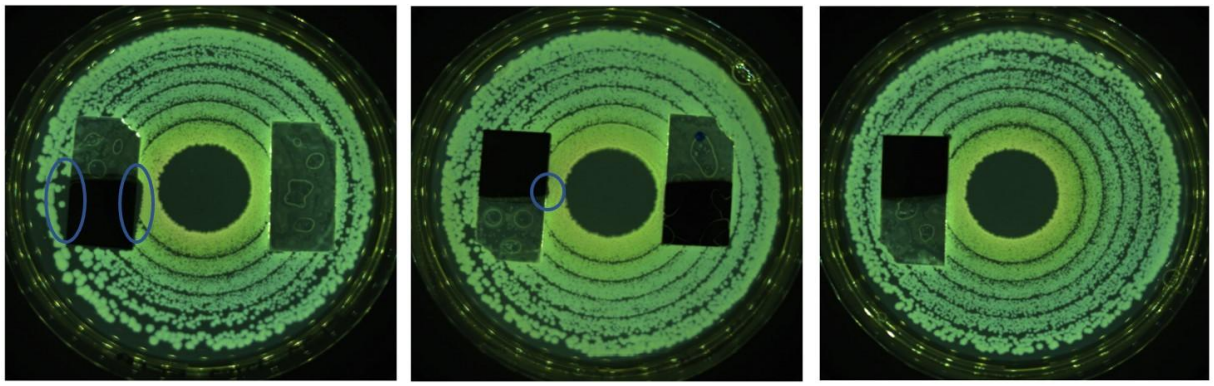

PPyZn-100 **TMSP-FTO** **PPyZn-50** **PPy** **PPyZn-10**

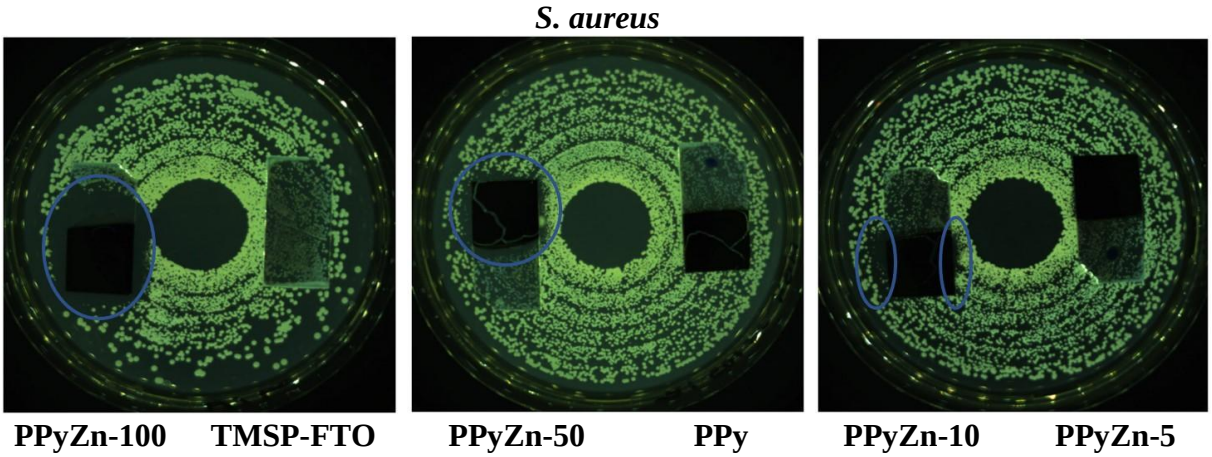

Figure 11. Comparison of inhibition zone assays obtained with PPyZn-films, PPy and TMSP-FTO substrates obtained with *E. coli* and *S. aureus*.

The bactericidal activity of our films was further studied by time-killing assays. To ensure that we only evaluated the bactericidal activity of our compounds, we used 100% phosphate-buffered saline (PBS) medium condition in which the quantity of CFUs remains constant during the whole procedure. We determined the percentages of surviving bacteria in the presence of all different films. As shown in Figure 12, for *E. coli*, polypyrrole film presents antibacterial properties with 46% of surviving bacteria after 6 hours. As mentioned in the introduction, polypyrrole is well known for its bactericidal activity that has been attributed to the strong electrostatic interactions between the positive charges along the polymer structure and the negatively charged bacterial cell wall.[61] Several papers have reported good antibacterial properties of polypyrrole obtained via chemical polymerization[25, 28] or electrodeposition[62-65] against *E. coli* and *S. aureus* with the highest efficiency against the former one. As expected, all PPy-Zn films present better antibacterial activities than the pure polypyrrole one. Indeed, for *E. coli*, the bacterial survival in the case of PPyZn-10 decreased to 17% after 6 hours. When the concentration of [PyC_8MIm]Br-$ZnCl_2$ is further increased to 50 mM no *E. coli* bacterial survived after 2 hours (PPyZn-50) and they are totally immediately killed in the presence of the PPyZn-100 film. These results are in line with the qualitative results obtained from inhibition zone assays. In the case of *S. aureus*, the film PPyZn-5 is very efficient and kills all bacteria within 150 min while all bacteria are immediately killed in the presence of the PPyZn-50 film. Looking now at the PPy film, its activity is as expected, lower against *S. aureus* than against *E. coli*.

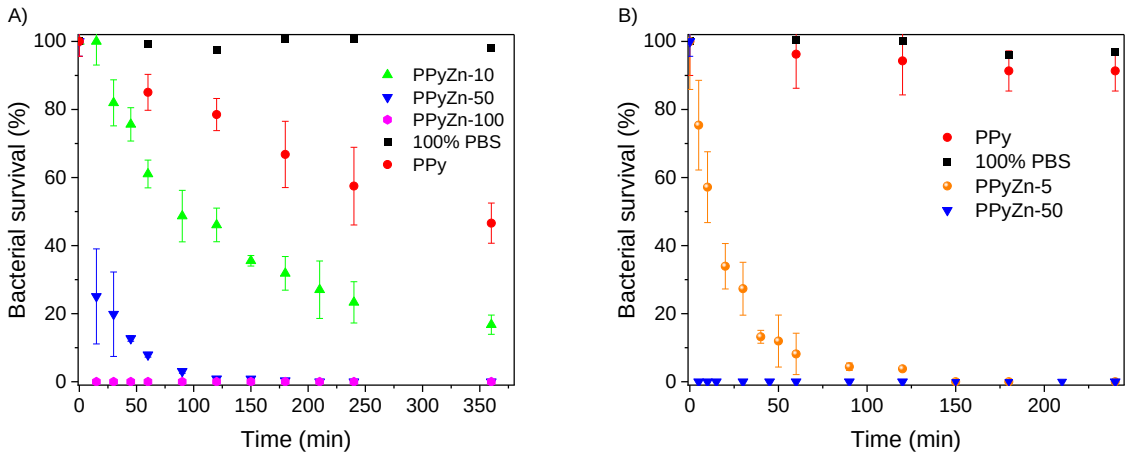

Figure 12. % of surviving (A) *E. coli* bacteria (B) *S. aureus* bacteria in the presence of the PPy films.

CONCLUSION

Antibacterial surfaces were prepared by co-electropolymerization of pyrrole and pyrrole-functionalized imidazolium IL bearing halometallate anion $[PyC_8MIm]Br\text{-}ZnCl_2$ on FTO substrate. Several films were prepared by tuning the concentration of $[PyC_8MIm]Br\text{-}ZnCl_2$. An efficient adhesion of polypyrrole films was obtain thanks to the pre-organosilanisation of the FTO substrates with *N*-[3-(trimethoxysilyl)propyl]pyrrole. XPS analyses confirmed the incorporation of the pyrrole-functionalized imidazolium component into the films and the formation of polynuclear $[Zn_nCl_{2n+1}Br]^{2-}$ anions. The morphology of the resulting films depend on the concentration of $[PyC_8MIm]Br\text{-}ZnCl_2$ used. While a classical nodular structure of polypyrrole is obtained at the lowest $[PyC_8MIm]Br\text{-}ZnCl_2$ concentration, the highest one present bigger polypyrrole aggregates that are surrounded by the alkyl imidazolium non-conducting organic component. The films thicknesses are in the range 7.4-8.9 µm. Investigation of the antibacterial properties by MIC determination of the monomer evidences that it presents higher antibacterial efficiency against Gram-positive *S. aureus* than against Gram-negative *E. coli*. The antibacterial properties of the films were also determined by too different technic, inhibition zone assay and time-killing experiments. The films present good antibacterial properties much higher than polypyrrole alone. In line with the antibacterial property of the monomer, the films possess higher antibacterial efficiency against *S. aureus*. More interestingly, we demonstrate that bacterial killing can be easily

modulated by a careful choice of the concentration of $[PyC_8MIm]Br\text{-}ZnCl_2$ used for the electropolymerization.

We are currently pushing further this study and investigate the effect of the monomer alkyl chain lengths on these antibacterial properties.

ASSOCIATED CONTENT

Supporting Information. ^{1}H, $^{13}C\{^{1}H\}$ NMR spectra and Infra-Red spectra for all compounds (PDF). The following file is available free of charge.

Author Contributions

The manuscript was written through contributions of all authors. All authors have given approval to the final version of the manuscript.

Funding Sources

This research was funded the Regional Council of Bourgogne Franche-Comté through the Envergure Program MatElectroCap.

ACKNOWLEDGMENT

The authors would like to thank Virginie Moutarlier for her help with GDOES analyses.

REFERENCES

1. Curreri, A. M.; Mitragotri, S.; Tanner, E. E. L., Recent Advances in Ionic Liquids in Biomedicine. *Adv. Sci.* **2021,** *8* (17), 2004819.
2. Fujita, K.; MacFarlane, D. R.; Forsyth, M., Protein solubilising and stabilising ionic liquids. *Chem. Commun.* **2005,** (38), 4804-4806.
3. Huang, W.; Wu, X.; Qi, J.; Zhu, Q.; Wu, W.; Lu, Y.; Chen, Z., Ionic liquids: green and tailor-made solvents in drug delivery. *Drug Discov. Today* **2020,** *25* (5), 901-908.
4. Pernak, J.; Sobaszkiewicz, K.; Mirska, I., Anti-microbial activities of ionic liquids. *Green Chem.* **2003,** *5* (1), 52-56.
5. Costa, F. M. S.; Saraiva, M. L. M. F. S.; Passos, M. L. C., Ionic liquids and organic salts with antimicrobial activity as a strategy against resistant microorganisms. *J. Mol. Liq.* **2022,** *368*, 120750.

6. Borkowski, A.; Gutowski, Ł.; Syczewski, M.; Cłapa, T.; Czerwonka, G., Adaptation of bacteria Escherichia coli in presence of quaternary ammonium ionic liquids. *Ecotoxicol. Environ. Saf.* **2018,** *164*, 370-378.
7. Borkowski, A.; Kowalczyk, P.; Czerwonka, G.; Cieśla, J.; Cłapa, T.; Misiewicz, A.; Szala, M.; Drabik, M., Interaction of quaternary ammonium ionic liquids with bacterial membranes – Studies with Escherichia coli R1–R4-type lipopolysaccharides. *J. Mol. Liq.* **2017,** *246*, 282-289.
8. Lovejoy, K. S.; Corley, C. A.; Cope, E. K.; Valentine, M. C.; Leid, J. G.; Purdy, G. M.; Wilkes, J. S.; Koppisch, A. T.; Del Sesto, R. E., Utilization of Metal Halide Species Ambiguity to Develop Amorphous, Stabilized Pharmaceutical Agents As Ionic Liquids. *Cryst. Growth Des.* **2012,** *12* (11), 5357-5364.
9. Gilmore, B. F.; Andrews, G. P.; Borberly, G.; Earle, M. J.; Gilea, M. A.; Gorman, S. P.; Lowry, A. F.; McLaughlin, M.; Seddon, K. R., Enhanced antimicrobial activities of 1-alkyl-3-methyl imidazolium ionic liquids based on silver or copper containing anions. *New J. Chem.* **2013,** *37* (4), 873-876.
10. de la Fuente-Nunez, C.; Brown, P.; Torres, M. D. T.; Cao, J.; Lu, T. K., Magnetic Surfactant Ionic Liquids and Polymers With Tetrahaloferrate (III) Anions as Antimicrobial Agents With Low Cytotoxicity. *Colloids Interface Sci. Commun.* **2018,** *22*, 11-13.
11. Muñoz-Bonilla, A.; Fernández-García, M., Poly(ionic liquid)s as antimicrobial materials. *Eur. Polym. J.* **2018,** *105*, 135-149.
12. Xu, Q.; Zheng, Z.; Wang, B.; Mao, H.; Yan, F., Zinc Ion Coordinated Poly(Ionic Liquid) Antimicrobial Membranes for Wound Healing. *ACS Appl. Mater. Inter.* **2017,** *9* (17), 14656-14664.
13. Zheng, Z.; Guo, J.; Mao, H.; Xu, Q.; Qin, J.; Yan, F., Metal-Containing Poly(ionic liquid) Membranes for Antibacterial Applications. *ACS Biomater. Sci. Eng.* **2017,** *3* (6), 922-928.
14. Ye, Q.; Gao, T.; Wan, F.; Yu, B.; Pei, X.; Zhou, F.; Xue, Q., Grafting poly(ionic liquid) brushes for anti-bacterial and anti-biofouling applications. *J. Mater. Chem.* **2012,** *22* (26), 13123-13131.
15. Yuan, Y.; Shang, Y.; Zhou, Y.; Guo, J.; Yan, F., Enabling Antibacterial and Antifouling Coating via Grafting of a Nitric Oxide-Releasing Ionic Liquid on Silicone Rubber. *Biomacromolecules* **2022,** *23* (6), 2329-2341.
16. Jin, L.; Shi, Z.; Zhang, X.; Liu, X.; Li, H.; Wang, J.; Liang, F.; Zhao, W.; Zhao, C., Intelligent antibacterial surface based on ionic liquid molecular brushes for bacterial killing and release. *J. Mater. Chem. B* **2019,** *7* (36), 5520-5527.
17. Liu, W.; Dong, Y.; Liu, S.; Wei, T.; Wu, Z.; Chen, H., Enhancement of Bactericidal Activity via Cyclic Poly(cationic liquid) Brushes. *Macromol. Rapid Commun.* **2019,** *40* (21), 1900379.
18. Pang, L. Q.; Zhong, L. J.; Zhou, H. F.; Wu, X. E.; Chen, X. D., Grafting of ionic liquids on stainless steel surface for antibacterial application. *Colloids Surf., B* **2015,** *126*, 162-168.
19. Dong, Y.; Wang, P.; Wei, T.; Zhou, T.; Huangfu, M.; Wu, Z., Smart Antibacterial Surfaces Established by One-Step Photo-Crosslinking. *Adv. Mater.* **2017,** *4* (24), 1700953.
20. Zeglio, E.; Rutz, A. L.; Winkler, T. E.; Malliaras, G. G.; Herland, A., Conjugated Polymers for Assessing and Controlling Biological Functions. *Adv. Mater.* **2019,** *31* (22), 1806712.
21. Kaur, G.; Adhikari, R.; Cass, P.; Bown, M.; Gunatillake, P., Electrically conductive polymers and composites for biomedical applications. *RSC Adv.* **2015,** *5* (47), 37553-37567.

22. Nezakati, T.; Seifalian, A.; Tan, A.; Seifalian, A. M., Conductive Polymers: Opportunities and Challenges in Biomedical Applications. *Chem. Rev.* **2018,** *118* (14), 6766-6843.
23. Wang, X.; Gu, X.; Yuan, C.; Chen, S.; Zhang, P.; Zhang, T.; Yao, J.; Chen, F.; Chen, G., Evaluation of biocompatibility of polypyrrole in vitro and in vivo. *J. Biomed. Mater. Res. A* **2004,** *68A* (3), 411-422.
24. Varesano, A.; Aluigi, A.; Florio, L.; Fabris, R., Multifunctional cotton fabrics. *Synth. Met.* **2009,** *159* (11), 1082-1089.
25. Varesano, A.; Vineis, C.; Tonetti, C.; Mazzuchetti, G.; Bobba, V., Antibacterial property on Gram-positive bacteria of polypyrrole-coated fabrics. *J. Appl. Polym. Sci.* **2015,** *132* (12).
26. Silva Júnior, F. A. G. d.; Vieira, S. A.; Botton, S. d. A.; Costa, M. M. d.; Oliveira, H. P. d., Antibacterial activity of polypyrrole-based nanocomposites: a mini-review. *Polímeros* **2020,** *30*, e2020048.
27. Ignatova, M.; Labaye, D.; Lenoir, S.; Strivay, D.; Jérôme, R.; Jérôme, C., Immobilization of Silver in Polypyrrole/Polyanion Composite Coatings: Preparation, Characterization, and Antibacterial Activity. *Langmuir* **2003,** *19* (21), 8971-8979.
28. da Silva Jr, F. A. G.; Queiroz, J. C.; Macedo, E. R.; Fernandes, A. W. C.; Freire, N. B.; da Costa, M. M.; de Oliveira, H. P., Antibacterial behavior of polypyrrole: The influence of morphology and additives incorporation. *Mater. Sci. Eng., C* **2016,** *62*, 317-322.
29. Gniadek, M.; Wichowska, A.; Antos-Bielska, M.; Orlowski, P.; Krzyzowska, M.; Donten, M., Synthesis and characterization of polypyrrole and its composites coatings on flexible surface and its antibacterial properties. *Synth. Met.* **2020,** *266*, 116430.
30. Sadki, S.; Schottland, P.; Brodie, N.; Sabouraud, G., The mechanisms of pyrrole electropolymerization. *Chem. Soc. Rev.* **2000,** *29* (5), 283-293.
31. Zhang, W.; Cui, J.; Lin, C.; Wu, Y.; Ma, L.; Wen, Y.; Li, G., Pyrrole containing ionic liquid as tecton for construction of ordered mesoporous silica with aligned polypyrrole nanowires in channels. *J. Mater. Chem.* **2009,** *19* (23), 3962-3970.
32. Chatterjee, P.; Nofen, E. M.; Xu, W.; Hom, C.; Jiang, H.; Dai, L. L., Pyrrole-based poly(ionic liquids) as efficient stabilizers for formation of hollow multi-walled carbon nanotubes particles. *J. Colloid Interface Sci.* **2017,** *504*, 140-148.
33. Zhang, W.; Li, Y.; Lin, C.; An, Q.; Tao, C.; Gao, Y.; Li, G., Electrochemical polymerization of imidazolum-ionic liquids bearing a pyrrole moiety. *J. Polym. Sci., Part A: Polym. Chem.* **2008,** *46* (12), 4151-4161.
34. Chen, H.; Anderson, J. L.; Anand, R. K., Electropolymerization of Pyrrole-Based Ionic Liquids on Selected Wireless Bipolar Electrodes. *ACS Appl. Mater. Inter.* **2022,** *14* (16), 18087-18096.
35. Devasurendra, A. M.; Zhang, C.; Young, J. A.; Tillekeratne, L. M. V.; Anderson, J. L.; Kirchhoff, J. R., Electropolymerized Pyrrole-Based Conductive Polymeric Ionic Liquids and Their Application for Solid-Phase Microextraction. *ACS Appl. Mater. Inter.* **2017,** *9* (29), 24955-24963.
36. Fairley, N.; Fernandez, V.; Richard- Plouet, M.; Guillot-Deudon, C.; Walton, J.; Smith, E.; Flahaut, D.; Greiner, M.; Biesinger, M.; Tougaard, S.; Morgan, D.; Baltrusaitis, J., Systematic and collaborative approach to problem solving using X-ray photoelectron spectroscopy. *Applied Surface Science Advances* **2021,** *5*, 100112.
37. Sougueh, C. M.; Lakard, S.; Husson, J.; Contal, E.; Monney, S.; Moutarlier, V.; Magnenet, C.; Lakard, B., Influence of pre-grafted pyrrole-based silane on the electrodeposition and chemical properties of polypyrrole films. *Synth. Met.* **2018,** *246*, 220-229.

38. Boullanger, S.; Contal, E.; Buron, C. C.; Viau, L., Pyrrole-tailed imidazolium surface-active monomers: aggregation properties in aqueous solution and polymerization behavior. *J. Mol. Liq.* **2022,** *350*, 118588.
39. Xie, H.-Q.; Liu, C.-M.; Guo, J.-S., Preparation of conductive polypyrrole composites by in-situ polymerization. *Polym. Int.* **1999,** *48* (11), 1099-1107.
40. Myers, R. E., Chemical oxidative polymerization as a synthetic route to electrically conducting polypyrroles. *J. Electron. Mater.* **1986,** *15* (2), 61-69.
41. Jayakumar, R.; Rajkumar, M.; Nagendran, R.; Nanjundan, S., Synthesis and characterization of metal-containing polyurethanes with antibacterial activity. *J. Appl. Polym. Sci.* **2002,** *85* (6), 1194-1206.
42. Estager, J.; Nockemann, P.; Seddon, K. R.; Swadźba-Kwaśny, M.; Tyrrell, S., Validation of Speciation Techniques: A Study of Chlorozincate(II) Ionic Liquids. *Inorg. Chem.* **2011,** *50* (11), 5258-5271.
43. Liu, Y.; Wu, G.; Qi, M., Polymorphous crystals from chlorozincate-choline chloride ionic liquids in different molar ratios. *J. Cryst. Growth* **2005,** *281* (2), 616-622.
44. Lecocq, V.; Graille, A.; Santini, C. C.; Baudouin, A.; Chauvin, Y.; Basset, J. M.; Arzel, L.; Bouchu, D.; Fenet, B., Synthesis and characterization of ionic liquids based upon 1-butyl-2,3-dimethylimidazolium chloride/ZnCl2. *New J. Chem.* **2005,** *29* (5), 700-706.
45. Alves, M. B.; Santos jr., V. O.; Soares, V. C. D.; Suarez, P. A. Z.; Rubim, J. C., Raman spectroscopy of ionic liquids derived from 1-n-butyl-3-methylimidazolium chloride and niobium chloride or zinc chloride mixtures. *J. Raman Spectrosc.* **2008,** *39* (10), 1388-1395.
46. Taylor, A. W.; Men, S.; Clarke, C. J.; Licence, P., Acidity and basicity of halometallate-based ionic liquids from X-ray photoelectron spectroscopy. *RSC Adv.* **2013,** *3* (24), 9436-9445.
47. Viau, L.; Hihn, J. Y.; Lakard, S.; Moutarlier, V.; Flaud, V.; Lakard, B., Full characterization of polypyrrole thin films electrosynthesized in room temperature ionic liquids, water or acetonitrile. *Electrochim. Acta* **2014,** *137*, 298-310.
48. Patois, T.; Lakard, B.; Monney, S.; Roizard, X.; Fievet, P., Characterization of the surface properties of polypyrrole films: Influence of electrodeposition parameters. *Synth. Met.* **2011,** *161* (21), 2498-2505.
49. Hashimoto, H.; Ohno, A.; Nakajima, K.; Suzuki, M.; Tsuji, H.; Kimura, K., Surface characterization of imidazolium ionic liquids by high-resolution Rutherford backscattering spectroscopy and X-ray photoelectron spectroscopy. *Surf. Sci.* **2010,** *604* (3), 464-469.
50. Lovelock, K. R. J.; Villar-Garcia, I. J.; Maier, F.; Steinrück, H.-P.; Licence, P., Photoelectron Spectroscopy of Ionic Liquid-Based Interfaces. *Chem. Rev.* **2010,** *110* (9), 5158-5190.
51. Kang, E. T.; Neoh, K. G.; Ong, Y. K.; Tan, K. L.; Tan, B. T. G., X-ray photoelectron spectroscopic studies of polypyrrole synthesized with oxidative iron(III) salts. *Macromolecules* **1991,** *24* (10), 2822-2828.
52. M, B.; Mathew, A. T.; K B, A.; Sirimahachai, U.; Varghese, A.; Hegde, G., Influence of electrochemical co-deposition of bimetallic Pt–Pd nanoclusters on polypyrrole modified ITO for enhanced oxidation of 4-(hydroxymethyl) pyridine. *RSC Adv.* **2022,** *12* (27), 17036-17048.
53. Docherty, K. M.; Kulpa, J. C. F., Toxicity and antimicrobial activity of imidazolium and pyridinium ionic liquids. *Green Chem.* **2005,** *7* (4), 185-189.
54. Cornellas, A.; Perez, L.; Comelles, F.; Ribosa, I.; Manresa, A.; Garcia, M. T., Self-aggregation and antimicrobial activity of imidazolium and pyridinium based ionic liquids in aqueous solution. *J. Colloid Interface Sci.* **2011,** *355* (1), 164-171.

55. Łuczak, J.; Jungnickel, C.; Łącka, I.; Stolte, S.; Hupka, J., Antimicrobial and surface activity of 1-alkyl-3-methylimidazolium derivatives. *Green Chem.* **2010,** *12* (4), 593-601.
56. Zheng, L.; Li, J.; Yu, M.; Jia, W.; Duan, S.; Cao, D.; Ding, X.; Yu, B.; Zhang, X.; Xu, F.-J., Molecular Sizes and Antibacterial Performance Relationships of Flexible Ionic Liquid Derivatives. *J. Am. Chem. Soc.* **2020,** *142* (47), 20257-20269.
57. Forero-Doria, O.; Araya-Maturana, R.; Barrientos-Retamal, A.; Morales-Quintana, L.; Guzmán, L., N-alkylimidazolium Salts Functionalized with p-Coumaric and Cinnamic Acid: A Study of Their Antimicrobial and Antibiofilm Effects. *Molecules* **2019,** *24* (19), 3484.
58. Venkata Nancharaiah, Y.; Reddy, G. K. K.; Lalithamanasa, P.; Venugopalan, V. P., The ionic liquid 1-alkyl-3-methylimidazolium demonstrates comparable antimicrobial and antibiofilm behavior to a cationic surfactant. *Biofouling* **2012,** *28* (10), 1141-1149.
59. Santos, A. G.; Ribeiro, B. D.; Alviano, D. S.; Coelho, M. A. Z., Toxicity of ionic liquids toward microorganisms interesting to the food industry. *RSC Adv.* **2014,** *4* (70), 37157-37163.
60. Weyhing-Zerrer, N.; Gundolf, T.; Kalb, R.; Oßmer, R.; Rossmanith, P.; Mester, P., Predictability of ionic liquid toxicity from a SAR study on different systematic levels of pathogenic bacteria. *Ecotoxicol. Environ. Saf.* **2017,** *139*, 394-403.
61. Zare, E. N.; Agarwal, T.; Zarepour, A.; Pinelli, F.; Zarrabi, A.; Rossi, F.; Ashrafizadeh, M.; Maleki, A.; Shahbazi, M.-A.; Maiti, T. K.; Varma, R. S.; Tay, F. R.; Hamblin, M. R.; Mattoli, V.; Makvandi, P., Electroconductive multi-functional polypyrrole composites for biomedical applications. *Appl. Mater. Today* **2021,** *24*, 101117.
62. Mîndroiu, M.; Ungureanu, C.; Ion, R.; Pîrvu, C., The effect of deposition electrolyte on polypyrrole surface interaction with biological environment. *Appl. Surf. Sci.* **2013,** *276*, 401-410.
63. Ungureanu, C.; Pirvu, C.; Mindroiu, M.; Demetrescu, I., Antibacterial polymeric coating based on polypyrrole and polyethylene glycol on a new alloy TiAlZr. *Prog. Org. Coat.* **2012,** *75* (4), 349-355.
64. Nautiyal, A.; Qiao, M.; Cook, J. E.; Zhang, X.; Huang, T.-S., High performance polypyrrole coating for corrosion protection and biocidal applications. *Appl. Surf. Sci.* **2018,** *427*, 922-930.
65. El Jaouhari, A.; El Asbahani, A.; Bouabdallaoui, M.; Aouzal, Z.; Filotás, D.; Bazzaoui, E. A.; Nagy, L.; Nagy, G.; Bazzaoui, M.; Albourine, A.; Hartmann, D., Corrosion resistance and antibacterial activity of electrosynthesized polypyrrole. *Synth. Met.* **2017,** *226*, 15-24.

For Table of Contents Only